Current Research in Microbial Sciences 7 (2024) 100270

Contents lists available at ScienceDirect

Current Research in Microbial Sciences

journal homepage: www.sciencedirect.com/journal/current-research-in-microbial-sciences

Integrating *In-silico* and *In-vitro* approaches to identify plant-derived bioactive molecules against spore coat protein CotH3 and high affinity iron permease FTR1 of *Rhizopus oryzae*

Lovely Gupta [a], Pawan Kumar [b], Pooja Sen [a], Aniket Sharma [a,c], Lokesh Kumar [a], Abhishek Sengupta [a], Pooja Vijayaraghavan [a,*]

[a] Amity Institute of Biotechnology, Amity University Uttar Pradesh, Sector-125, Noida, 201301, Uttar Pradesh, India
[b] School of Computational and Integrative Sciences, Jawaharlal Nehru University, New Delhi, India
[c] Department of Animal Science, University of Wyoming, Laramie, WY, 82071, USA

ARTICLE INFO

Keywords:
Bioactive molecules
CotH3
FTR1
Rhizopus oryzae
Virulence

ABSTRACT

Rhizopus oryzae is one of the major causative agents of mucormycosis. The disease has a poor prognosis with a high mortality rate, and resistance towards current antifungal drugs poses additional concern. The disease treatment is complicated with antifungals; therefore, surgical approach is preferred in many cases. A comprehensive understanding of the pathogenicity-associated virulence factors of *R. oryzae* is essential to develop new antifungals against this fungus. Virulence factors in *R. oryzae* include cell wall proteins, spore germination proteins and enzymes that evade host immunity. The spore coat protein (CotH3) and high-affinity iron permease (FTR1) have been identified as promising therapeutic targets in *R. oryzae. In-silico* screening is a preferred approach to identify hit molecules for further *in-vitro* studies. In the present study, twelve bioactive molecules were docked within the active site of CotH3 and FTR1. Further, molecular dynamics simulation analysis of best-docked protein-ligand structures revealed the dynamics information of their stability in the biological system. Eugenol and isoeugenol exhibited significant binding scores with both the protein targets of *R. oryzae* and followed the Lipinski rule of drug-likeness. To corroborate the *in-silico* results, *in-vitro* studies were conducted using bioactive compounds eugenol, isoeugenol, and myristicin against *R. oryzae* isolated from the soil sample. Eugenol, isoeugenol exhibited antifungal activity at 156 μg/mL whereas myristicin at 312 μg/mL. Hence, the study suggested that eugenol and isoeugenol could be explored further as potential antifungal molecules against *R. oryzae.*

Introduction

Mucormycosis is a serious but rare fungal infection, is caused by a group of fungi belonging to the order *Mucorales*, with reported mortality rates ranging from 50 % to 100 % (Inglesfield et al., 2018). A higher mortality rate is observed in patients with neutropenia, solid organ transplants, iron overload, and uncontrolled diabetes mellitus (Petrikkos et al. 2012; Claustre et al. 2020). Globally, the prevalence of mucormycosis varies between 0.005 – 1.7 per million population; the reported prevalence in India was 0.14 per 1000 individuals in 2019–2020 (Chander et al. 2018; Skiada et al. 2020). India reported the highest burden of mucormycosis in patients with COVID-19 (Aranjani et al. 2021).

The most common causative agents of mucormycosis are *Rhizopus, Mucor*, and *Lichtheimia* species. *Rhizopus spp*. is the most common among them, which releases large numbers of airborne conidia. *Rhizopus oryzae* var *arrhizus* is the major *Rhizopus spp*. causing mucormycosis followed by *R. delemar, R. microspores, Mucor regularis,* and *Rhizomucor* (Chander et al. 2018; Prakash and Chakrabarti 2019). Various virulence factors are crucial in the *R. oryzae* infection process, including, spore coat protein (CotH), high-affinity iron permease (FTR1), alkaline *Rhizopus* protease enzyme (ARP), calcineurin, and serine and aspartate proteases (Ibrahim et al., 2010; Morales-Franco et al. 2021). Among these, spore coat protein homolog CotH3 has been detected exclusively on the spore surface of the order *Mucorales.* CotH3 plays a key role in invasion in the mucormycosis pathogenesis by disrupting and damaging immune cells

* Corresponding author.
E-mail address: vrpooja@amity.edu (P. Vijayaraghavan).

https://doi.org/10.1016/j.crmicr.2024.100270

Available online 23 August 2024

(Gebremariam et al. 2014). It's a kinase protein present on the surface of the conidia that promotes adhesion to the host endothelial cell surface through its binding to the glucose-regulator protein 78 (GRP78) during host cell invasion. When endothelial cells are exposed to acidosis and elevated levels of glucose and iron (in hyperglycemia and diabetes ketoacidosis), GRP78 expression increases, leading to fungal invasion and damage to endothelial cells in a receptor-dependent manner (Roilides et al. 2014). CotH3 gene and protein are prime targets to restrict the virulence of *R.oryzae* under hyperglycemia and other forms of acidosis.

In patients with diabetes ketoacidosis, treatment with iron deferoxamine increases iron availability, thereby increasing the risk for mucormycosis (Ibrahim and Kontoyiannis 2013). Virulence factor FTR1 has a crucial role in iron uptake and transportation at the time of infection. The acquisition of iron is a crucial pathogenic event for opportunistic fungi such as *R. oryzae* (Stanford and Voigt 2020). Different mechanisms of iron uptake have been reported in fungi. The reductive system of iron uptake involves activity of an external reductase of ferric iron and subsequently transportation by a complex of multicopper oxidase and ferrous permease (Knight et al. 2002; Fu et al. 2004). FTR1 and CotH3 proteins are highly conserved within the order *Mucorales*, thereby becoming promising drug targets for mucormycosis treatment.

The treatment of mucormycosis is compromised by a limited spectrum of effective antifungal drugs (https://www.cdc.gov/fungal/diseases/mucormycosis/treatment.html). Only three antifungal drugs are currently approved namely, lipid formulations of amphotericin B, posaconazole, and isavuconazole (Roemer and Krysan 2014). However, an alarming increase in resistant fungal strains and severe side effects of amphotericin B (hepatotoxicity, nephrotoxicity, and myelotoxicity) pose a severe challenge to therapeutic strategies (Dannaoui 2017; Sen et al. 2022). Therefore, new drug targets should be explored to develop safe and effective antifungals for the treatment of mucormycosis. Medicinal plants represent a vast source of new pharmacologically active molecules for the treatment of fungal diseases (Chathurdevi and Gowrie 2016; Adeleke and Babalola 2021). They are source of many active molecules including eugenol, isoeugenol, alpha-pinene, camphene, 1, 8-cineole, elemicin, limonene, methyl-eugenol, myristicin, and β-terpineol, with potential antimicrobial activities (Park et al. 2012; Torbati et al. 2014; Şimşek and Duman 2017).

In-silico approach is a knowledge-based method that helps to select bioactive molecules with a high likelihood of biological activity. The approach can focus on the molecules with relevant biological effects directly retrieved from the published literature (Rollinger et al. 2009). Docking study proposes protein-ligand binding characteristics; and the ligand that performs significantly *in-silico* activity can be used as a promising starting molecule for the *in-vitro* experimental work, preferably by target binding assays. The present study aimed to screen bioactive compounds against virulence proteins CotH3 and FTR1 of *R. oryzae via in-silico* approach, and *in-vitro* evaluation of antifungal activity of bioactive compounds eugenol, isoeugenol, and myristicin.

Materials and methods

Preparation of ligands

The identified molecules listed in Table S1 were originally derived from the hexane extract of *Myristica fragrans* (Hoda et al. 2020) and were selected based on their reported bioactivity (Kuete 2017; Hoda et al. 2020); The 3D chemical structures of 12 selected bioactive molecules were retrieved from the PubChem database (https://www.ncbi.nlm.nih.gov/pmc/articles/PMC4702940/) in Spatial Data File (SDF) format. Using OpenBabel tool, input file of ligands in the SDF file format (.sdf) was converted to the PDB file formats (.pdb) for molecular docking (O'Boyle et al. 2011).

Search for the target sequence, structures, and preparation

The protein sequences of CotH3 (accession no KAG1547117.1) and FTR1 (accession no AAQ24109.1) of *R. oryzae* were retrieved from NCBI (https://www.ncbi.nlm.nih.gov/). As their 3D structures were not available in the Protein Data Bank (PDB), homology modelling was conducted using Swiss Model via ExPasy web server (https://swissmodel.expasy.org/) with template alignment. Tertiary structures of modelled protein were evaluated using PROCHECK software. Modelled protein structures were further prepared using Swiss PDB viewer (SPDBV-4.10) version with charge assignment, solvation parameters and fragmental volumes (https://spdbv.unil.ch/). The protein molecules were further optimized using AutoDock4 Tool for the molecular docking (Morris et al., 2009).

Molecular docking

The docking analysis was performed by molecular docking program AutoDock4.2.3 software (Morris et al. 2009). The grid box (60 × 60 × 60) was set to cover the whole protein. Docking calculations were carried out with the Lamarckian genetic algorithm. The total number of docking runs was set to 50 with other default values during each docking run. Poses were further clustered utilizing all-atom root mean square deviation (RMSD) cut-off of 0.3 Å to remove redundancy with an average 20 cluster representatives. The protein structure was inflexible at all steps. All the docking poses and interaction analysis were produced via Discovery Studio Visualizer programs (Şimşek and Duman 2017).

Absorption, distribution, metabolism, excretion, and toxicity (ADME-Tox) profile prediction

The ADME-Tox profiles of selected molecules were predicted by SwissADME program (http://www.swissadme.ch/index.php; Sharma et al. 2020). The major ADME-Tox properties parameters taken in this study were: molecular weight, H-bond acceptor, H-bond donors, predicted octanol/water partition coefficient (MLogP), rotatable bonds, topological polar surface area (TPSA), blood brain barrier (BBB) permeant and oral bioavailability score.

Molecular dynamics (MD) simulation and analysis

MD simulation was performed using GROMACS software to analyze conformational dynamics of the unbound and bound state of FTR1 and CotH3 protein. GROMOS force field (Schmid et al. 2011) was used for protein and PRODRG web-server (http://davapc1.bioch.dundee.ac.uk/cgi-bin/prodrg/) was used to parametrised the ligand molecules during simulation. The cubic simulation box of 10 Å was prepared considering the protein at center, and the box was filled with TIP3P water molecules (Pekka and Nilsson 2001) for solvation under periodic boundary conditions. Some water molecules were replaced by counter ions to neutralize systems. Particle Mesh Ewald (PME) method was used for calculating all electrostatic interactions and 2 fs time step was used with the SHAKE algorithm to constrain the hydrogen bonds.

The simulation box was initially minimized for 500,000 steps using the steepest descent and conjugate gradient methods. The system was then gradually heated from 0 to 300 K in six stages, followed by a 1 ns equilibration run under NVT ensemble. The final 100 ns production run was conducted under NPT ensemble with an integration time step of 2.0 fs. Trajectories were saved every 100 ps and analysed using GROMACS trajectory module for the RMSD, root mean square fluctuation (RMSF), and solvent accessible surface areas (SASA) (Lindahl et al. 2001).

Fungal isolation, its molecular characterization and antifungal susceptibility

Ten soil samples were collected from various agricultural fields in the

Haryana region and stored in sterile polythene bags. Soil samples were processed and inoculated on potato dextrose agar (PDA) following the method described by Sen et al. (2023). Inoculated PDA plates were then incubated at 28 ± 2 °C for 5 days, and fungal growth was observed. All samples were processed in biological triplicate. Fungal isolates were identified based on morphological and microscopic characteristics using standard mycological reference charts (Dugan 2012; Barnett and Hunter 2006). The identified *Rhizopus* isolate was subcultured and subjected to molecular identification. The full-length 18S internal transcribed spacer (ITS) region was amplified using the universal primers ITS1 and ITS4 (White et al., 1990) and the PCR-amplified ITS region was sequenced by Sanger's sequencing. The obtained sequences were compared to the sequences in the GenBank database (www.ncbi.nlm.nih.gov.in) using BLAST analysis, and identification was confirmed when a sequence identity of 99–100 % was observed. Minimum inhibitory concentration (MIC) of eugenol, isoeugenol, myristicin and triazole drugs itraconazole, voriconazole, posaconazole and polyene antifungal amphotericin B against *R. oryzae* was determined by using CLSI M38-A2 broth micro-dilution method (Alexander 2017). Two-fold dilutions were carried out in a 96-well microplate to obtain concentrations ranging from 32 to 0.0625 µg/mL for itraconazole, voriconazole, posaconazole, and amphotericin B; 5000- 9.76 µg/mL for eugenol, isoeugenol, and myristicin. The growth in each well was compared with that of the positive control; the plate was incubated at 28 ± 2 °C for 5 days. The experiment was conducted in triplicates. The MIC is defined as the lowest concentration of the compound, which completely inhibits microbial growth (Alexander 2017). The results were expressed in micrograms per milliliters (µg/mL).

Statistical analysis

For the statistical analysis, one sample *t*-test was used to analyse the MIC values of antifungal drugs and bioactive compounds tested against *R. oryzae*. All experiments were conducted in biological duplicates and technical triplicates. Statistics were performed using GraphPad Prism software 8.0.2.263 version.

Results

Homology model of R. oryzae CotH3 and FTR1 and its accuracy assessment

R. oryzae CotH3 and FTR1 proteins were modelled via SwissModel. The 3D structure of CotH3 was modelled based on the template PDB ID 5JD9 (Fig.1A), while FTR1 was modelled using template PDB ID 4JR9 chain A (Fig. 1C). To assess the stereo-chemical quality and accuracy of the models, PROCHECK was employed and results were presented in Ramachandran plots (Fig. 1B and 1D). For CotH3, 84.3 % of residues were in the most favoured regions, 14.6 % residues in additional allowed regions, and only 0.6 % residues in disallowed regions. Similarly, in the FTR1 protein, 85.1 % of residues were in the most favoured regions, 12.3 % residues were in additional allowed regions and no residues were found in disallowed regions. Overall, the homology-modelled proteins demonstrated good quality based on the Ramachandran plot analysis.

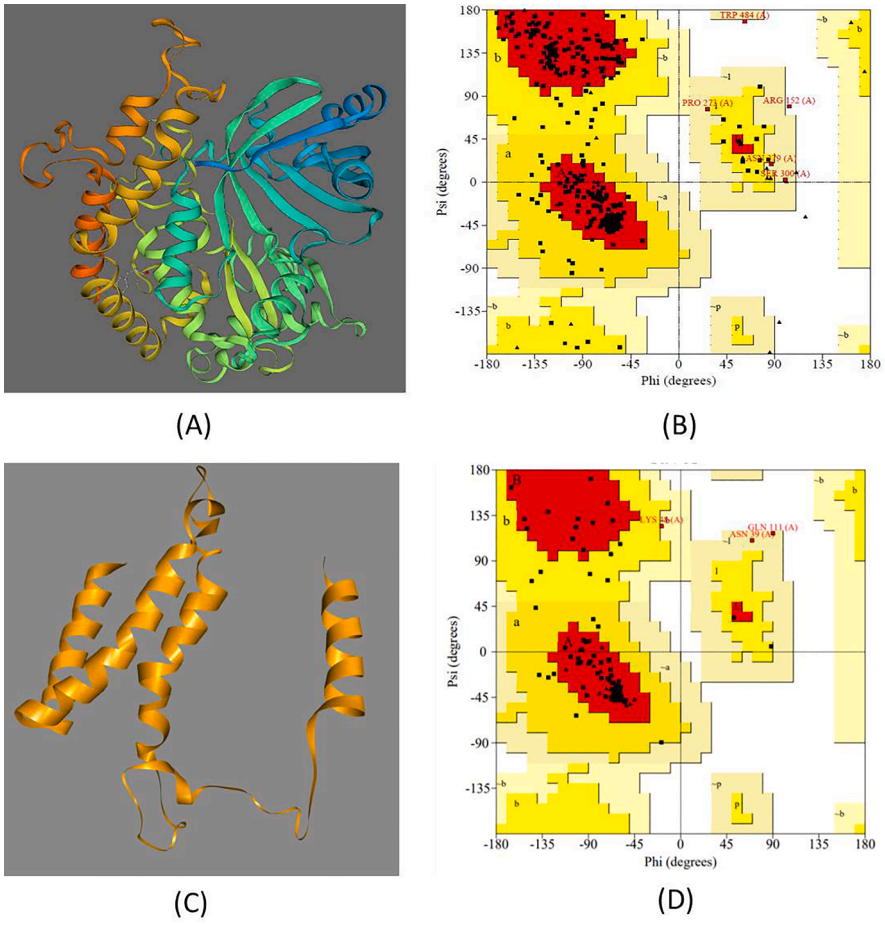

Fig. 1. Ribbon structure of the spore coat protein CotH3 (A) and high-affinity iron permease FTR1 (C) of *Rhizopus oryzae*; and Ramachandran plot analysis of CotH3 (B) and FTR1 (D). Filled black squares are all non-glycine and proline residues, filled black triangles are all glycine (non-end) and disallowed residues are red portions.

Molecular docking

Molecular docking was performed to evaluate the interaction of 12 plant-derived molecules having antimicrobial activity with CotH3 and FTR1 proteins of *R. oryzae*. The docking was directed at the reported catalytic site of CotH3 protein where it binds to GRP78 host receptor during infection. The amino acid residue present at the docking pocket was Met364. The coordinates of Met364 residue were x-axis: 21.766, y-axis: 51.757, and z-axis: 29.357. For FTR1 protein, blind docking was employed to evaluate the probable binding site for ligands. The strategy of AutoDock4- based blind docking included a search over the entire surface of the protein for binding sites. The binding affinities of short-listed molecules at the active site were assessed. The docking scores are listed in Table S2 along with their interactions.

Interactions of 12 bioactive molecules with the active site of CotH3 were analysed using AutoDock4. The best docking score of −6.93 Kcal/mol with three hydrogen bonds (Val 420 and Met 421) (Fig. 2) was given by myristicin at the catalytic site of CotH3 protein followed by isoeugenol (−6.89 Kcal/mol). In addition, eugenol and methyl-eugenol exhibited binding affinity of −6.75 Kcal/mol and −6.60 Kcal/mol, respectively. Eugenol formed two hydrogen bonds (Val 420, and Met 421), and methyl eugenol formed three hydrogen bonds: two with Val 420 and one with Met 421 (Fig. 2). Isoeugenol with more negative binding affinity formed four hydrogen bonds (two with Val 420, one with Met 364 and one with Met 421) at the catalytic site of CotH3 of *R. oryzae* (Fig. 2). The catalytic site of CotH3 possesses amino acids Met 364, Gln 366, which forms hydrogen bond and show van der Waal interaction with the eugenol, isoeugenol, methyl-eugenol and myristicin. β-Terpineol formed only one hydrogen bond with a docking score of −5.95 Kcal/mol, which is a very low binding affinity at the catalytic site. Limonene, elemicin, 1,8-cineole, camphene, and α-pinene displayed binding affinities of −6.06, −6.38, −5.73, −5.90 Kcal/mol and −5.50 Kcal/mol, respectively. However, these compounds did not form any hydrogen bonds at the active site of CotH3. Linoleic acid and oleic acid showed a low binding affinity with less negative docking score.

The binding affinity was reduced for the FTR1 protein, although all molecules docked at the same predicted active site on the protein. The highest binding affinity was shown by β-terpineol (−5.6 Kcal/mol) followed by eugenol and isoeugenol (−5.43 and −5.46 Kcal/mol, respectively; Fig. 3). Eugenol and isoeugenol formed one hydrogen bond at the predicted active site with Thr 61, whereas β-terpineol formed one hydrogen bond with Leu 49. Elemicin, methyl-eugenol, myristicin, linoleic acid, and oleic acid binding affinities were −5.21 Kcal/mol, −5.22 Kcal/mol, −5.30 Kcal/mol, −5.39 Kcal/mol and −5.33 Kcal/mol, respectively. Linoleic and oleic acids formed two hydrogen bonds with Ala 32, Leu 31 and Trp 27, Lys 33, respectively. Limonene showed a binding affinity of −5.04 Kcal/mol but did not form any conventional hydrogen bond. Camphene, 1,8-cineole, and α-pinene gave negative binding affinity below −5.00 Kcal/mol and, were not considered for further analysis.

ADME-Tox profile prediction

The ADME-Tox study of five selected molecules (eugenol, isoeugenol, methyl-eugenol, β-terpineol, and myristicin) was evaluated for

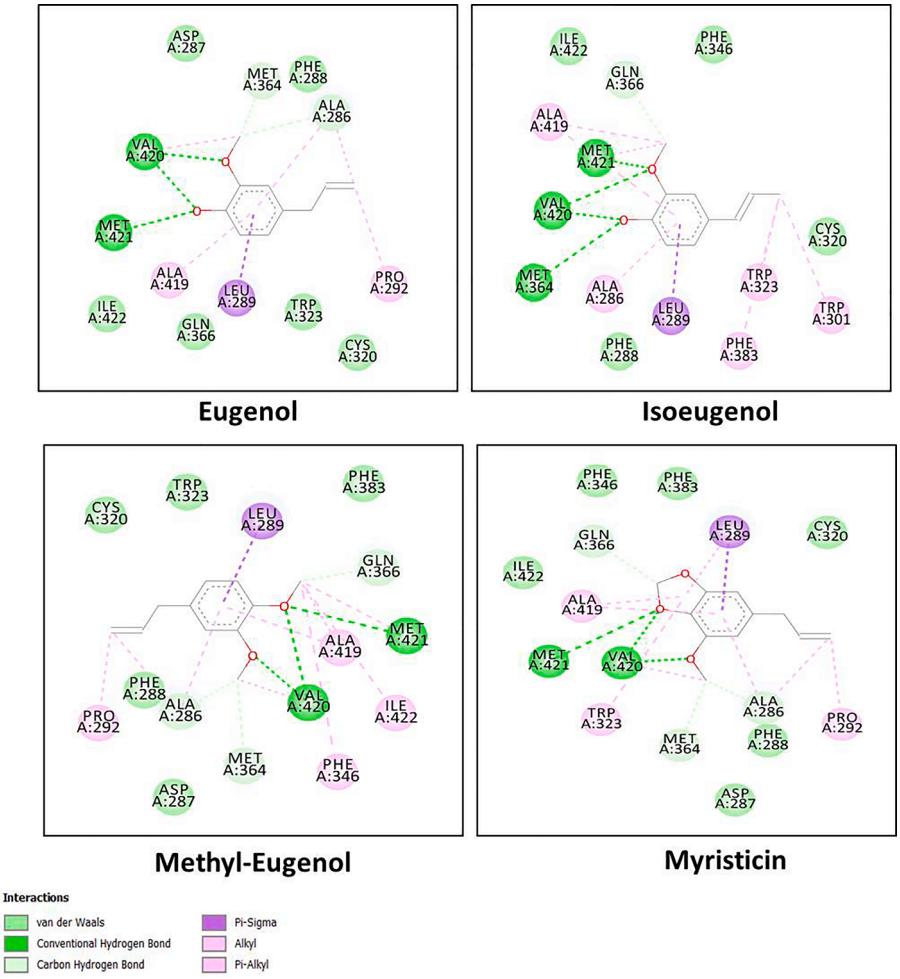

Fig. 2. Binding interactions of eugenol, isoeugenol, methyl-eugenol, and myristicin with the active site of CotH3 protein of *Rhizopus oryzae*.

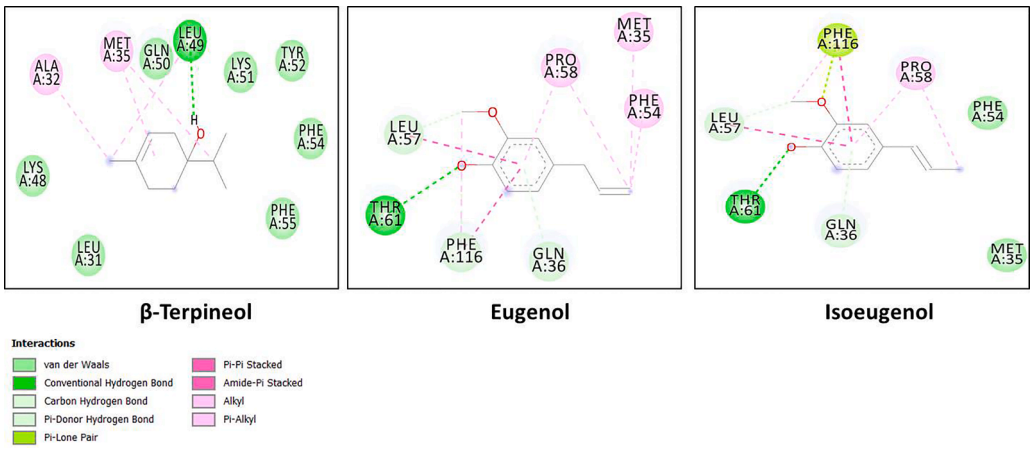

Fig. 3. Binding interactions of β-Terpineol, eugenol and isoeugenol with the active site of FTR1 protein of *Rhizopus oryzae*.

their drug-likeness properties. Table 1 lists key criteria for a molecule to possess drug-like properties *via* oral route. All the molecules had molecular weight <500 g mol^{-1}, MlogP value <5, rotatable bonds <10, and TPSA <140$Å^2$. Only methyl eugenol and myristicin did not possess hydrogen bond donors; eugenol, isoeugenol, and β-terpineol followed Lipinski's rule of five, Veber and Egan's rules. None of the studied molecules violated the drug likeness properties. Gastrointestinal absorption and brain access are two more crucial pharmacokinetic properties to determine a molecule as drug candidate. In relation, the BOILED-Egg predictive model showed all molecules in the yellow region, with the highest probability of permeating to the brain. The oral bioavailability score for all molecules was 0.55.

Molecular dynamics simulation

MD simulation was performed for 100 ns simulation time for six systems which included three from CotH3 and three from FTR1 (only receptor and two docked ligand-protein complex). Based on the binding affinities and ADME-Tox parameters, eugenol and isoeugenol ligands were selected for further MD simulation studies.

The RMSD (Fig. 4A and B) and SASA (Fig. 4E and F) trajectories were calculated to assess the protein-ligand stability in the presence of a bound ligand while RMSF (Fig. 4C and D) was employed to understand the average fluctuation of protein residues. Fig. 4 displays the RMSD, RMSF and SASA plots for CotH3 and FTR1 systems. RMSD distribution for eugenol-bound CotH3 complex is relatively higher than the receptor only (Fig. 4A). The probing showed that the major contribution in fluctuation was of the coiled secondary structure situated at the N-terminal side of the protein. The RMSF plot (Fig. 4C) displayed that 50–200 amino acid region have very high fluctuation compared to receptor-only for that region. We have further investigated the docked ligand position in the CotH3 binding site. For both CotH3 complexes, SASA is nearly consistent till 100 ns duration whereas in case of FTR1 complex, it gets reflected after eugenol binding depicting some conformational changes (Fig. 4E and F). Centre-mean distance between docked ligands and binding site residue (Trp 323) was calculated and Fig. S1 demonstrated that eugenol and isoeugenol remained in the binding site of the protein and after 100 ns simulation, the distance plot for both complexes plateaued with very minimum deviation. Results suggested that eugenol and isoeugenol bound CotH3 complexes achieved stability, despite relatively high RMSD deviation which is mainly of coiled secondary structure.

In case of FTR1 complexes, FTR1 model structure has four helices, three helices clustered together while the fourth helix is connected with coiled secondary structure (17–50 residues) with the rest helices. Due to the flexibility incorporated by the >30 residues long coiled region, this region and attached helix do not directly engage with the binding of the docked ligands. So, we have recalculated the RMSD after excluding the 1–50 residues from both complexes and Fig. S2 shows the RMSD plot for 51–130 region. This calculation reflects that both complexes are very well stable and do not show much deviation upon ligand binding. Hence, CotH3 and FTR1 docked complexes are stable and can be used for further understanding.

Isolation of R. oryzae, its molecular identification and antifungal susceptibility

Among all ten soil samples processed, only one *Rhizopus* isolate was identified based on its morphological and microscopic characteristics (Fig 5). The sequences obtained from amplification of conserved ribosomal ITS region were compared with BLAST Programme on NCBI. The sequence was identified as *R. oryzae* and submitted in the GenBank (Accession number OQ868363). MIC of eugenol and isoeugenol was found to be 156 μg/mL whereas MIC of myristicin was calculated as 312 μg/mL. MIC of itraconazole, voriconazole, posaconazole and amphotericin B was 4 μg/mL, 32 μg/mL, 2 μg/mL, and 16 μg/mL, respectively (Fig. 6).

Discussion

Rhizopus causes pulmonary infections in patients with hematologic malignancies, and it also causes rhino orbital/cerebral mucormycosis in

Table 1
Physicochemical and drug-likeness properties of CotH3 and FTR1 protein inhibitors determined by SwissADME.

Bioactive molecules	Molecular Formula	Molecular weight (g mol^{-1})	LogP	H-bond donor	H-bond acceptor	Rotatable bonds	TPSA	Molar refractivity	Violation* of Lipinski, Veber, Egan's rule
Eugenol	$C_{10}H_{12}O_2$	164.20	2.25	1	2	3	29.46$Å^2$	49.06	No
Isoeugenol	$C_{10}H_{12}O_2$	164.20	2.41	1	2	2	29.46$Å^2$	49.86	No
Methyl Eugenol	$C_{11}H_{14}O_2$	178.23	2.58	0	2	4	18.46$Å^2$	53.53	No
Myristicin	$C_{11}H_{12}O_3$	192.21	2.49	0	3	3	27.69$Å^2$	53.10	No
β-Terpineol	$C_{10}H_{18}O$	154.25	2.44	1	1	1	20.23$Å^2$	48.80	No

* Molecular weight (<500 g mol^{-1}), LogP (<5), H-bond donor (<5), H-bond acceptor (<10), Rotatable bonds (<10), Topological polar surface area (TPSA <140$Å^2$).

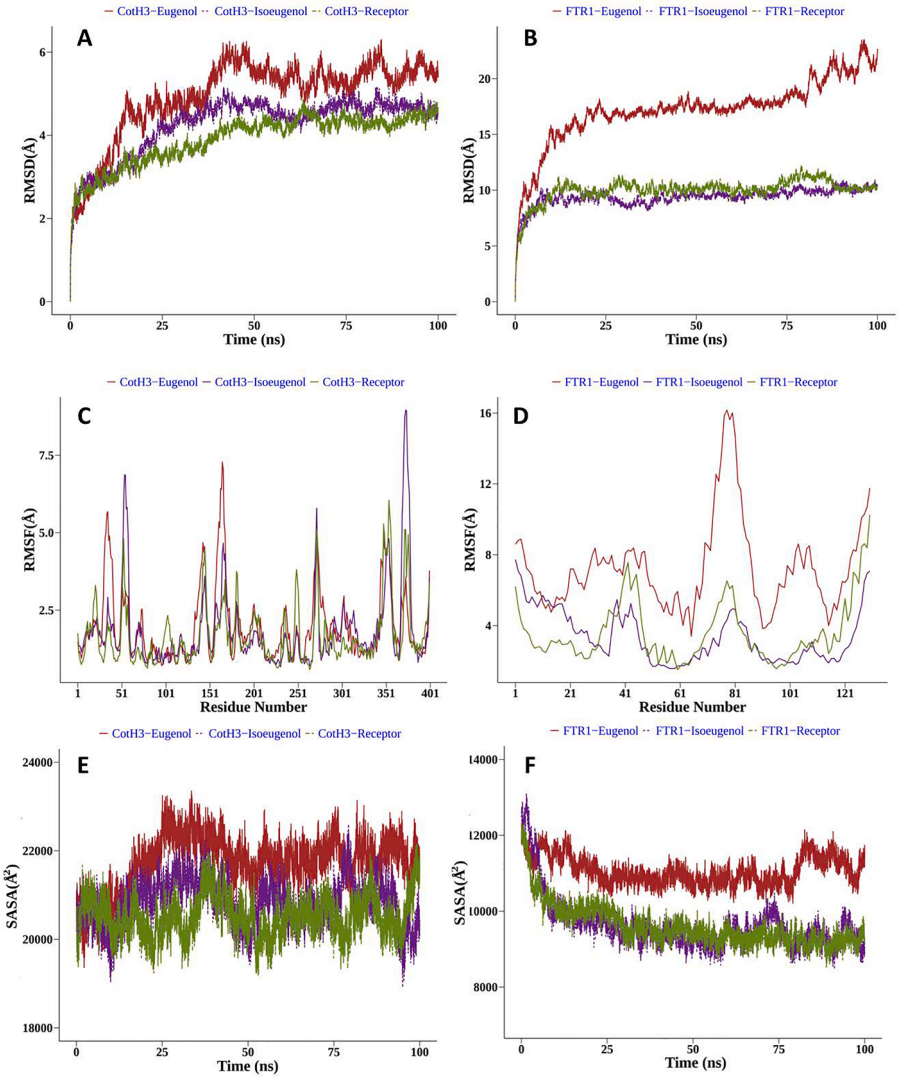

Fig. 4. Root Mean Square Deviation RMSD values of complexes during 100 ns MD simulations (A,B); Root Mean Square Fluctuation RMSF (C,D), and Solvent Accessible Surface Areas SASA (E,F) plots of the CotH3 and FTR1 of *Rhizopusoryzae*.

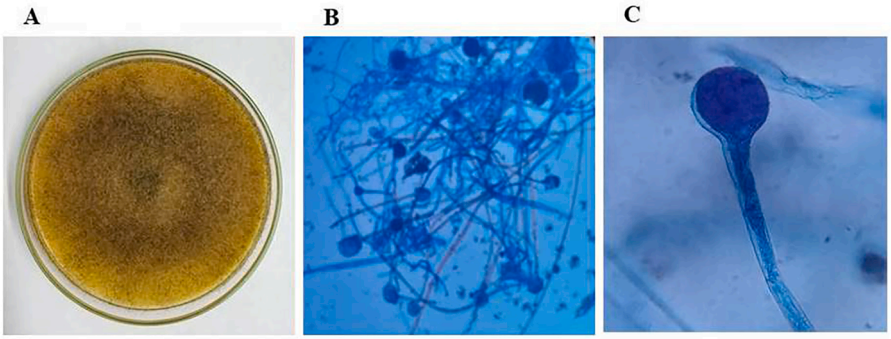

Fig. 5. *Rhizopus oryzae* colony morphology on potato dextrose agar (A) and microscopic images 40X (B) and 100X (C) magnifications.

patients suffering from diabetic ketoacidosis (DKA). Elevated concentrations of glucose, iron, and ketone bodies, which occur in patients with hyperglycemia and DKA, enhance GRP78 and CotH3 expression, leading to augmented fungal invasion and damage in the host cell. *R. oryzae* thrives under high glucose and acidic conditions and interacts with the host cell receptor GRP78 *via* CotH3 (Liu et al. 2010; Gebremariam et al. 2014). CotH proteins are present in *Mucorales* but are absent in other medically important fungi such as *Aspergillus* and *Candida*. These proteins are the prime targets for mucormycosis, which have not been studied in detail.

In the present study, homology modelling was performed to retrieve 3D structure of CotH3 protein *via* Swiss-model web server. The CotH3 protein has multiple α-helical domains which provide a structural scaffold to it. However, the protein in its secondary structure differs

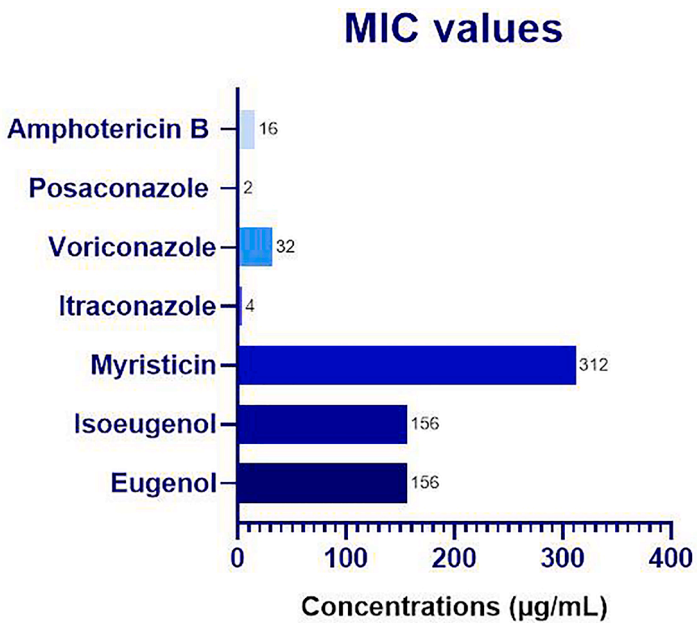

Fig. 6. Graphical representation of Minimum inhibitory concentrations (MICs; µg/mL) of current antifungal drugs (Amphotericin B, Posaconazole, Voriconazole and Itraconazole) and bioactive compounds (Myristicin, Isoeugenol and eugenol) against *R. oryzae* isolate.

considerably in the extent of its β-sheet conformation (Gebremariam et al. 2014). The CotH3 exhibited an extended docking-predicted GRP78 contact point, with minimal β-sheet stabilization. The amino acid sequence MGQTNDGAYRDPTDNN of CotH3 is a highly conserved sequence used to raise antibodies in mouse model. The antibodies inhibited endothelial cell invasion in vitro and protected mice against mucormycosis. In the present study, molecular docking was performed using CotH3 protein as a target and twelve bioactive molecules as ligands, selected from our previous study. The current study showed, that out of twelve listed molecules, myristicin, eugenol, isoeugenol and methyl-eugenol interacted at the active site of CotH3 protein with negative binding energy and formed at least two hydrogen bonds at the binding site. The binding affinity revealed the interaction and strength by which a compound interacts with and binds to the active site of the target protein. Compounds having binding affinity of −6.5 Kcal/mol or less are considered good inhibitors of enzymatic activities (Shah et al. 2020).

High iron affinity system is identified as a key molecular virulence determinant, which contains ferric reductase, ferroxidase and permease (Hassan and Voigt 2019). FTR1 protein was also evaluated as another crucial virulence factor of *R. oryzae*. This system reduces free ferric ion by ferric reductase to obtain a more soluble iron form. The reduced iron is again oxidised by ferroxidase and is recognised by FTR1 protein which in the end concedes the transport inside the cell (Navarro-Mendoza et al. 2018). It is also regulated by the environmental level of iron and is activated when there is low availability of it in the surrounding environment. Lack of iron has been shown to reduce virulence, trigger growth defects, and induce apoptosis in the *R. oryzae* (Ibrahim and Kontoyiannis 2013). Since there was no data available for the active site of the FTR1 protein, blind docking was conducted to find the binding efficiency of plant-derived molecules with the protein. In the current study, the binding affinity between FTR1 and ligands was not significant but all the docked ligands found same active site on the protein i.e., Thr 61 residue. The ligand β-terpineol followed by eugenol and isoeugenol showed binding affinity of −5.60, −5.43 and −5.46 Kcal/mol, respectively. The lowest autodock binding energy and best interactions were used to ascertain the compound with the best conformation (Vikram and Mishra 2018; Kamboj et al. 2022).

In the present study, eugenol and isoeugenol displayed binding affinities with CotH3 and FTR1. The chemical structure of eugenol and isoeugenol differ in the position of the double bond in the propene side chain (Koeduka et al. 2008). Isoeugenol interacted with CotH3 protein binding site forming 4 hydrogen bonds, whereas eugenol formed 2 hydrogen bonds, having similar binding affinity. Further, MD simulation was conducted to examine the dynamical stability of the CotH3 and FTR1 receptor protein in the presence of the docked ligands. In the case of CotH3 complexes, CotH3-eugenol complex attended more RMSD and SASA values along the simulation time compared with CotH3-isoeugenol complex and CotH3 receptor itself. However, further trajectory analysis showed that coiled secondary structure was mainly responsible for this higher RMSD and in both CotH3 complexes; docked ligands remain stable on the proposed binding site. In case of FTR1 complexes, FTR1-eugenol complex achieved more RMSD compared to FTR1-isoeugenol complex. N-terminal helix connects with other helices along with nearly 30 residues long random coiled structure and this was found to be a major determinant in high RMSD in case of FTR1-eugenol complex. Excluding this region during RMSD calculation showed both complexes are well stable during 100 ns simulation. This simulation result further suggested that docked ligand molecules stabilise both receptor complexes.

Docking studies suggested that eugenol and isoeugenol exhibited efficacy against both the target virulence proteins of *R. oryzae*. The phenolic compounds can express their antifungal effect by targeting host-pathogen adhesion, reducing the fluidity of the membrane, and inhibiting cell wall synthesis or energy metabolism (Gupta et al. 2018; Donadio et al. 2021). Eugenol and isoeugenol interfere with microbial membrane functions or suppress virulence factors (toxins, and enzymes involves in various biosynthetic pathways), and inhibit biofilm formation (Gupta et al. 2022). MIC of eugenol and isoeugenol was 156 µg/mL against *R. oryzae,* which is lower than MIC reported against filamentous fungi *Aspergillus fumigatus* (Gupta et al. 2022). Natural sources are being actively investigated because of their importance in drug discovery (Newman and Cragg 2012; Atanasov et al. 2021). For drug development processes, complete knowledge of the interaction of a drug candidate with its molecular target is useful. As per the literature, structural modifications in the bioactive compounds would lead to enhance the drug efficacy and reduce their side-effects (Goswami et al. 2022).

Mucorales typically exhibit intrinsic resistance to certain antifungal drugs (itraconazole, fluconazole (Diflucan), voriconazole) (Caramalho et al. 2017) and there is very limited data related to their antifungal

susceptibility and MIC values of antifungals (Espinel-Ingroff et al. 2015; Sipsas et al. 2018; Yousfi et al. 2019; Dogra et al. 2022). This significantly restricts the options for antifungal treatments. In the present study, *R. oryzae* isolate demonstrated resistance to amphotericin B, while showing susceptibility to posaconazole. There were high MIC values of voriconazole and itraconazole against *R. oryzae* isolate, which supports the intrinsic resistance to voriconazole and itraconazole that has previously been documented.

A good pharmacokinetics property plays an important role in the new drug candidate that should be evaluated in the process of drug development (Can et al. 2017). The ADME-Tox study of eugenol, isoeugenol, methyl-eugenol, β-terpineol, and myristicin displayed no violations of Lipinski's rule of five, Veber's rule and Egan's rule (Veber et al., 2002). BBB index was in favor of oral bioavailability of molecules and BBB permeation of compounds showed evidence for brain penetration which lies inside the yellow region of BOILED egg model. The BOILED egg model depicted the predictive power of gastrointestinal absorption and brain permeation (Daina and Zoete 2016). Furthermore, *in-silico* prediction of ADME properties of compounds that fall within the range could be used to evaluate the suitability of compounds as potential drugs.

Conclusion

In conclusion, this study identifies eugenol and isoeugenol as potential antifungal molecules against *R. oryzae*. Through *in-silico* screening and MD simulations, both molecules exhibited significant binding scores with key virulence factors CotH3 and FTR1, while adhering to drug-likeness criteria. *In-vitro* studies further confirmed their antifungal activity. These findings highlight the promise of eugenol and isoeugenol as potential therapeutic options for combating mucormycosis. Nevertheless, additional research and clinical investigations are essential to fully understand their efficacy and safety profiles, ultimately paving the way for novel and effective antifungal treatments against this life-threatening infection.

Author's contributions

LG, AS and PS conducted literature search, performed experiments and drafted the manuscript; PK and AS performed molecular dynamics and simulations analysis; LK conducted the fungi identification and PV conceptualised the idea and critically analysed the results and manuscript.

Declaration of competing interest

The authors declare that they have no known competing financial interests or personal relationships that could have appeared to influence the work reported in this paper.

Data availability

Authors have mentioned the link in the attached manuscript file.

Supplementary materials

Supplementary material associated with this article can be found, in the online version, at doi:10.1016/j.crmicr.2024.100270.

References

Adeleke, B.S., Babalola, O.O., 2021. Pharmacological potential of fungal endophytes associated with medicinal plants: a review. J. Fungi (Basel) 7, 147. https://doi.org/10.3390/jof7020147.

Alexander, B.D., 2017. Clinical and Laboratory Standards Institute.Reference method For Broth Dilution Antifungal Susceptibility Testing of Filamentous Fungi. CLSI standard M38, Pennsylvania USA, 3rd ed.

Aranjani, J.M., Manuel, A., Razack, H.I.A., Mathew, S.T., 2021. COVID-19–associated mucormycosis: evidence-based critical review of an emerging infection burden during the pandemic's second wave in India. PLoS Negl. Trop. Dis. 15, e0009921 https://doi.org/10.1371/journal.pntd.0009921.

Atanasov, A.G., Zotchev, S.B., Dirsch, V.M., et al., 2021. Natural products in drug discovery: advances and opportunities. Nature Rev. Drug Discov. 20, 200–216. https://doi.org/10.1038/s41573-020-00114-z.

Barnett, H.L., Hunter, B.B., 2006. Illustrated Genera of Imperfect Fungi. The American Phytopatological Society, St. Paul Minnesota, p. 234.

Can, N.Ö., Acar, Ç.U., Sağlık, B.N., et al., 2017. Synthesis, molecular docking studies, and antifungal activity evaluation of new benzimidazole-triazoles as potential lanosterol 14 α -demethylase inhibitors. J. Chem. Sci. 2017 1–15. https://doi.org/10.1155/2017/9387102.

Caramalho, R., Tyndall, J.D.A., Monk, B.C., et al., 2017. Intrinsic short-tailed azole resistance in mucormycetes is due to an evolutionary conserved aminoacid substitution of the lanosterol 14α-demethylase. Sci. Rep. 7, 15898. https://doi.org/10.1038/s41598-017-16123-9.

Chander, J., Kaur, M., Singla, N., et al., 2018. Mucormycosis: battle with the deadly enemy over a five-year period in India. J. Fungi (Basel) 4, E46. https://doi.org/10.3390/jof4020046.

Chathurdevi, G., Gowrie, S.U., 2016. Endophytic fungi isolated from medicinal plant-a promising source of potential bioactive metabolites. Int. J. Curr. Pharmaceutical Res. 8 (1), 50–56.

Claustre, J., Larcher, R., Jouve, T., et al., 2020. Mucormycosis in intensive care unit: surgery is a major prognostic factor in patients with hematological malignancy. Ann. Intensive Care 10, 74. https://doi.org/10.1186/s13613-020-00673-9.

Daina, A., Zoete, V., 2016. A BOILED-Egg to predict gastrointestinal absorption and brain penetration of small molecules. ChemMedChem. 11, 1117–1121.

Dannaoui, E., 2017. Antifungal resistance in mucorales. Int. J. Antimicrob. Agents 50, 617–621. https://doi.org/10.1016/j.ijantimicag.2017.08.010.

Dogra, S., Arora, A., Aggarwal, A., et al., 2022. Mucormycosis Amid COVID-19 crisis: pathogenesis, diagnosis, and novel treatment strategies to combat the spread. Front. Microbiol. 12, 794176 https://doi.org/10.3389/fmicb.2021.794176.

Donadio, G., Mensitieri, F., Santoro, V., et al., 2021. Interactions with microbial proteins driving the antibacterial activity of flavonoids. Pharmaceutics. 13, 660. https://doi.org/10.3390/pharmaceutics13050660.

Dugan, F.M., 2012. The Identification of fungi: An Illustrated Introduction with Keys, Glossary, and Guide to Literature. American Phytopathological Society, St. Paul, Minn, p. 176.

Espinel-Ingroff, A., Chakrabarti, A., Chowdhary, A., et al., 2015. Multicenter evaluation of MIC distributions for epidemiologic cutoff value definition to detect amphotericin B, posaconazole, and itraconazole resistance among the most clinically relevant species of Mucorales. Antimicrob. Agents Chemother. 59, 1745–1750. https://doi.org/10.1128/AAC.04435-14.

Fu, Y., Lee, H., Collins, M., et al., 2004. Cloning and functional characterization of the Rhizopus oryzae high affinity iron permease (rFTR1) gene. FEMS Microbiol. Lett. 235, 169–176. https://doi.org/10.1111/j.1574-6968.2004.tb09583.x.

Gebremariam, T., Liu, M., Luo, G., et al., 2014. CotH3 mediates fungal invasion of host cells during mucormycosis. J. Clin. Investig. 124, 237–250. https://doi.org/10.1172/JCI71349.

Goswami, L., Gupta, L., Paul, S., Vermani, M., Vijayaraghavan, P., Bhattacharya, A.K., 2022. Design and synthesis of eugenol/isoeugenol glycoconjugates and other analogues as antifungal agents against *Aspergillus fumigatus*. RSC. Med. Chem. 13, 955–962. https://doi.org/10.1039/d2md00138a.

Gupta, L., Sen, P., Bhattacharya, A.K., Vijayaraghavan, P., 2022. Isoeugenol affects expression pattern of conidial hydrophobin gene *RodA* and transcriptional regulators *MedA* and *SomA* responsible for adherence and biofilm formation in *Aspergillus fumigatus*. Arch. Microbiol. 204, 1–14. https://doi.org/10.1007/s00203-022-02817-w, 2022.

Gupta, P., Gupta, S., Sharma, M., et al., 2018. Effectiveness of Phytoactive Molecules on Transcriptional Expression, Biofilm Matrix, and Cell Wall Components of Candida glabrata and Its Clinical Isolates. ACS. Omega 3, 12201–12214. https://doi.org/10.1021/acsomega.8b01856.

Hassan, M.I.A., Voigt, K., 2019. Pathogenicity patterns of mucormycosis: epidemiology, interaction with immune cells and virulence factors. Med. Mycol. 57, S245–S256. https://doi.org/10.1093/mmy/myz011.

Hoda, S., Vermani, M., Joshi, R.K., et al., 2020. Anti-melanogenic activity of Myristica fragrans extract against *Aspergillus fumigatus* using phenotypic based screening. BMC. Complement. Med. Ther. 20, 67. https://doi.org/10.1186/s12906-020-2859-z.

Ibrahim, A.S., Kontoyiannis, D.P., 2013. Update on mucormycosis pathogenesis. Curr. Opin. Infect. Dis. 26, 508–515. https://doi.org/10.1097/QCO.0000000000000008.

Ibrahim, A.S., Teclegiorgis Gebremariam, T., Lin, L., et al., 2010. The high affinity iron permease is a key virulence factor required for *Rhizopus oryzae* pathogenesis. Mol. Microbiol. 77, 587–604. https://doi.org/10.1111/j.1365-2958.2010.07234.x.

Inglesfield, S., Jasiulewicz, A., Hopwood, M., Tyrrell, J., Youlden, G., Mazon-Moya, M., Millington, O.R., Mostowy, S., Jabbari, S., Voelz, K., 2018. Robust phagocyte recruitment controls the opportunistic fungal pathogen Mucor circinelloides in innate granulomas in vivo. mBio 9, e02010–e02017. https://doi.org/10.1128/mBio.02010-17.

Kamboj, H., Gupta, L., Kumar, P., et al., 2022. Gene expression, molecular docking, and molecular dynamics studies to identify potential antifungal compounds targeting virulence proteins/genes VelB and THR as possible drug targets against Curvularia

lunata. Front. Mol. Biosci. 9, 1055945 https://doi.org/10.3389/fmolb.2022.1055945.
Knight, S.A.B., Lesuisse, E., Stearman, R., et al., 2002. Reductive iron uptake by Candida albicans: role of copper, iron and the TUP1 regulator. Microbiology (N. Y) 148, 29–40. https://doi.org/10.1099/00221287-148-1-29.
Koeduka, T., Louie, G.V., Orlova, I., et al., 2008. The multiple phenylpropene synthases in both Clarkia breweri and Petunia hybrida represent two distinct protein lineages. Plant J. 54, 362–374. https://doi.org/10.1111/j.1365-313X.2008.03412.x.
Kuete, V., (2017). Chapter 23 - Myristica fragrans: a Review. In: Kuete V (ed) Medicinal Spices and Vegetables from Africa. Academic Press, pp 497–512.
Lindahl, E., Berk, H., David Van, S., 2001. GROMACS 3.0: a package for molecular simulation and trajectory analysis. Mol. Model. Annu. 7, 306–317.
Liu, M., Spellberg, B., Phan, Q.T., et al., 2010. The endothelial cell receptor GRP78 is required for mucormycosis pathogenesis in diabetic mice. J. Clin. Investig. 120, 1914–1924. https://doi.org/10.1172/JCI42164.
Morales-Franco, B., Nava-Villalba, M., Medina-Guerrero, E.O., et al., 2021. Host-pathogen molecular factors contribute to the pathogenesis of *rhizopus spp.* in diabetes mellitus. Curr. Trop. Med. Rep. 8, 6–17. https://doi.org/10.1007/s40475-020-00222-1.
Morris, G.M., Huey, R., Lindstrom, W., et al., 2009. AutoDock4 and AutoDockTools4: automated docking with selective receptor flexibility. J. Comput. Chem. 30, 2785–2791. https://doi.org/10.1002/jcc.21256.
Navarro-Mendoza, M.I., Pérez-Arques, C., Murcia, L., et al., 2018. Components of a new gene family of ferroxidases involved in virulence are functionally specialized in fungal dimorphism. Sci. Reports 8, 7660. https://doi.org/10.1038/s41598-018-26051-x.
Newman, D.J., Cragg, G.M., 2012. Natural products as sources of new drugs over the 30 years from 1981 to 2010. J. Nat. Prod. 75, 311–335. https://doi.org/10.1021/np200906s.
O'Boyle, N.M., Banck, M., James, C.A., et al., 2011. Open Babel: an open chemical toolbox. J. Cheminform. 3, 33. https://doi.org/10.1186/1758-2946-3-33.
Park, S.N., Lim, Y.K., Freire, M.O., et al., 2012. Antimicrobial effect of linalool and α-terpineol against periodontopathic and cariogenic bacteria. Anaerobe 18, 369–372. https://doi.org/10.1016/j.anaerobe.2012.04.001.
Petrikkos, G., Skiada, A., Lortholary, O., et al., 2012. Epidemiology and clinical manifestations of mucormycosis. Clin. Infectious Dis. 54 (Suppl 1), S23–S34. https://doi.org/10.1093/cid/cir866.
Prakash, H., Chakrabarti, A., 2019. Global epidemiology of mucormycosis. J. Fungi 5, 26. https://doi.org/10.3390/jof5010026.
Roemer, T., Krysan, D.J., 2014. Antifungal drug development: challenges, unmet clinical needs, and new approaches. Cold. Spring. Harb. Perspect. Med. 4, a019703 https://doi.org/10.1101/cshperspect.a019703.
Roilides, E., Antachopoulos, C., Simitsopoulou, M., 2014. Pathogenesis and host defence against Mucorales: the role of cytokines and interaction with antifungal drugs. Mycoses. 57 (Suppl 3), 40–47. https://doi.org/10.1111/myc.12236.
Rollinger, J.M., Schuster, D., Danzl, B., et al., 2009. In silico target fishing for rationalized ligand discovery exemplified on constituents of Ruta graveolens. Planta Med. 75, 195–204. https://doi.org/10.1055/s-0028-1088397.
Schmid, N., Eichenberger, A.P., Choutko, A., Riniker, S., Winger, M., Mark, A.E., van Gunsteren, W.F., 2011. Definition and testing of the GROMOS force-field versions 54A7 and 54B7. Eur. Biophys. J. 40, 843–856. https://doi.org/10.1007/s00249-011-0700-9.
Sen, P., Gupta, L., Vijay, M., Vermani, M.S., Shankar, J., Hameed, S., Vijayaraghavan, P., 2023. 4-Allyl-2-methoxyphenol modulates the expression of genes involved in efflux pump, biofilm formation and sterol biosynthesis in azole resistant *Aspergillus fumigatus*. Front. Cell Infect. Microbiol. 13, 1103957 https://doi.org/10.3389/fcimb.2023.1103957.
Sen, P., Vijay, M., Singh, S., Hameed, S., Vijayaragavan, P., 2022. Understanding the environmental drivers of clinical azole resistance in Aspergillus species. Drug Target. Insights 16, 25–35. https://doi.org/10.33393/dti.2022.2476.
Shah, B., Modi, P., Sagar, S.R., 2020. In silico studies on therapeutic agents for COVID-19: drug repurposing approach. Life Sci. 252, 117652 https://doi.org/10.1016/j.lfs.2020.117652.
Sharma, A., Goyal, S., Yadav, A.K., et al., 2020. In-silico screening of plant-derived antivirals against main protease, 3CLpro and endoribonuclease, NSP15 proteins of SARS-CoV-2. J. Biomol. Struct. Dyn. 40, 86–100. https://doi.org/10.1080/07391102.2020.1808077.
Şimşek, M., Duman, R., 2017. Investigation of Effect of 1,8-cineole on antimicrobial activity of chlorhexidine gluconate. Pharmacognosy. Res. 9, 234–237. https://doi.org/10.4103/0974-8490.210329.
Sipsas, N.V., Gamaletsou, M.N., Anastasopoulou, A., Kontoyiannis, D.P., 2018. Therapy of mucormycosis. J. Fungi 4, 90. https://doi.org/10.3390/jof4030090.
Skiada, A., Pavleas, I., Drogari-Apiranthitou, M., 2020. Epidemiology and diagnosis of mucormycosis: an update. J. Fungi 6, 265. https://doi.org/10.3390/jof6040265.
Stanford, F.A., Voigt, K., 2020. Iron assimilation during emerging infections caused by opportunistic fungi with emphasis on mucorales and the development of antifungal resistance. Genes. (Basel) 11, E1296. https://doi.org/10.3390/genes11111296.
Torbati, M., Nazemiyeh, H., Lotfipour, F., et al., 2014. Chemical composition and in vitro antioxidant and antibacterial activity of Heracleum transcaucasicum and Heracleum anisactis roots essential oil. Bioimpacts. 4, 69–74. https://doi.org/10.5681/bi.2014.004.
Veber, D.F., Johnson, S.R., Cheng, H.Y., Smith, B.R., Ward, K.W., Kopple, K.D., 2002. Molecular properties that influence the oral bioavailability of drug candidates. J. Med. Chem. 45, 2615–2623.
Vikram, S., Mishra, S., 2018. Molecular docking studies of benzamide derivatives for PfDHODH inhibitor as potent antimalarial agent. Am. J. Biochem. Mol. Biol. 9, 1–6. https://doi.org/10.3923/ajbmb.2019.1.6.
White, T.J., Bruns, T.D., Lee, S.B., Taylor, J., 1990. Amplification and direct sequencing of fungal ribosomal RNA genes for phylogenetics. A Guide to Methods and Applications. PCR protocols, San Diego, pp. 315–322.
Yousfi, H., Ranque, S., Rolain, J.-M., Bittar, F., 2019. In vitro polymyxin activity against clinical multidrug-resistant fungi. Antimicrobial Resistance Infect Control 8, 66. https://doi.org/10.1186/s13756-019-0521-7.